Experimental Investigation of Particle Pinch Associated with Turbulence in LHD Heliotron and JT-60U Tokamak Plasmas

K. Tanaka 1), H. Takenaga 2), K. Muraoka 3), C. Michael 4), L. N. Vyacheslavov 5), M. Yokoyama 1), H. Yamada 1), N. Oyama 2), H. Urano 2), Y. Kamada 2), S. Murakami 6), A. Wakasa 7), T. Tokuzawa 1), T. Akiyama 1), K. Kawahata 1), M. Yoshinuma1), K. Ida 1), I. Yamada 1), K. Narihara 1), N. Tamura 1) and the LHD experimental group 1)

1) National Institute for Fusion Science, Toki 509-5292, Japan
2) Japan Atomic Energy Agency, 801-1 Mukouyama, Naka, Ibaraki 311-0193, Japan
3) Chubu University, 1200 Matsumoto, Kasugai, Aichi 487-8501, Japan
4) EURATOM/UAKEA Fusion Association, Oxfordshire OX14 3 DB, United Kingdom
5) Budker Institute of Nuclear Physics, 630090, Novosibirsk, Russia
6) Department of Nuclear Engineering, Kyoto University, Kyoto 606-8501, Japan
7) Graduate School of Engineering, Sapporo Hokkaido University, 060-8628, Japan

e-mail contact of main author: ktanaka@LHD.nifs.ac.jp

Abstract. Comparative studies were carried out in LHD heliotron and JT-60U tokamak plasmas to elucidate the most essential parameter(s) for control of density profiles in toroidal systems. A difference in the collisionality dependence was found between the two devices. In LHD, the density peaking factor decreased with decrease of the collisionality at the magnetic axis position (R_{ax}) 3.6m, while the density peaking factor gradually increased with a decreased of collisionality at R_{ax}=3.5m. On the other hand, in JT-60U, the density peaking factor clearly increased with a decrease of the collisionality. The difference in the collisionality dependence between R_{ax}=3.5 and R_{ax}=3.6m is likely due to the contribution of the anomalous transport. At R_{ax}=3.5m, larger anomalous transport caused a similar collisionality dependence. Change of the fluctuation property was observed with different density profiles in the plasma core region on both devices. In JT-60U, the increase of the radial coherence was observed with higher density peaking profile suggesting enhanced diffusion and inward directed pinch. For a magnetic axis positions (R_{ax}) at 3.6m in LHD, the increase of the fluctuation power with an increase in P_{NB} was observed for a hollow density profile suggesting an increase on diffusion due to anomalous processes. Change of density profiles from peaked to hollow indicates change in the convection direction. This is due to increase in neoclassical processes. The reduction of the density peaking factor with increase of P_{NB} in LHD is partly due to the neoclassical effect and partly due to the anomalous effect.

1. Introduction

Understanding the physics mechanism of the electron density profile is one of the essential issues for the control of a future fusion reactor for both heliotron/stellarator and tokamak devices. Many experimental works and theoretical investigations suggest the role of neoclassical effects and turbulence. The neoclassical mechanism is driven by the collisions of confined particles and described by a well developed theoretical model. The main contributors to the turbulence mechanism are the ion temperature gradient mode (ITG) and the trapped electron mode (TEM). The neoclassical mechanism can account for experimentally observed profiles in both devices in limited operation regimes. However, in many other regimes, this mechanism is too weak to be responsible for the observed density profiles. Many theoretical models of anomalous particle transport were proposed, still, none of them can explain a number of experimental observations. In addition, the role of turbulence in building density profiles is not clear experimentally because measurements in the plasma core region are very limited. In this article, the responses of turbulent fluctuations caused by the change of density

profiles are compared for both devices.

2. General comparison of density profiles between JT60-U and LHD

Figure 1 shows radial profiles of electron density (n_e) and electron temperature (T_e) of JT-60U and LHD with neutral beam (NB) heating. The data of JT-60U is from the ELMy H mode. The data of LHD is from the L mode. However, the energy scaling of L mode in LHD is Gyro Bohm scaling as same as tokamak ELMy H mode scaling [1]. Clear differences in density profiles can be seen for the different densities in JT-60U and for the different R_{ax} in LHD. Particle sources from the walls decreased exponentially and did not affect the core density profiles (at $\rho<0.95$) in both devices. In JT-60U, the central particle source was changed by a factor of three by the combination of NB and electron cyclotron heating powers. However, the density peaking factor did not change [2]. In LHD, central particle fueling increased by a factor of eight with an increase of NB power at R_{ax}=3.6 m, resulting in changes in the density profiles from peaked to hollow although NB fueling supplied particles more to the core than to the edge [3]. Carbon impurity profiles did not change in both devices, indicating that impurity accumulation did not affect the density profiles. These suggest the changes in density profiles to be not due to the difference in particle fueling, but due to the differences in transport in both devices. In JT-60U, the contribution of the neoclassical Ware pinch was negligible, thus requiring the assumption of an anomalous inwardly directed pinch. As shown in Figs. 1 (a) and (b), the density profile in JT-60U is more peaked at a low value of n_e and/or a high value of T_e. This fact may indicate an anomalous inward pinch being larger with decreasing collisionality. In LHD, neoclassical transport is minimized by reducing the effective helical ripple at around R_{ax}=3.5-3.6 m [4] and has almost the same value for both positions. Therefore, the observed difference in density profiles is due to different contribution of anomalous transport for R_{ax} = 3.5 m and 3.6 m.

Figure 2 shows the dependence of density peaking factors on an electron-ion collision frequency normalized by the trapped electron bounce frequency (ν^*_b). The density peaking factor was defined as the ratio of the density at ρ=0.2 against the volume averaged density and ν^*_b was estimated at ρ=0.5. As shown in Fig. 2, density peaking factors increased with decreasing ν^*_b in JT-60U. The origin of density peaking in tokamaks is theoretically suggested as due to the turbulence-driven inward pinch, resulting in the increase of the

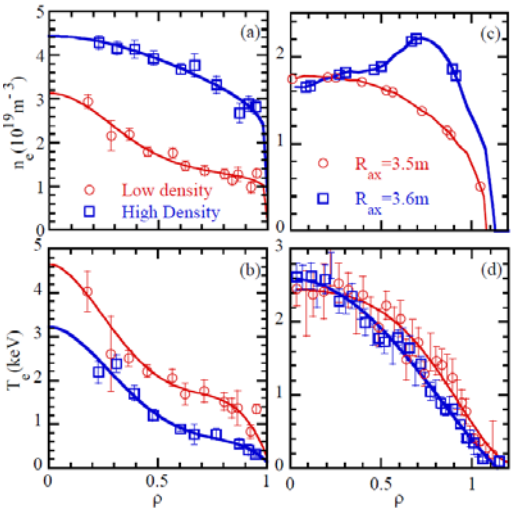

Fig. 1 (a), (c) n_e, and (b),(d) T_e profiles. (a) and (b) from JT-60U, and (c) and (d) from LHD. Here, plasmas in low and high density plasmas in JT-60U, and those at R_{ax}=3.5m and R_{ax}=3.6m in LHD are compared.

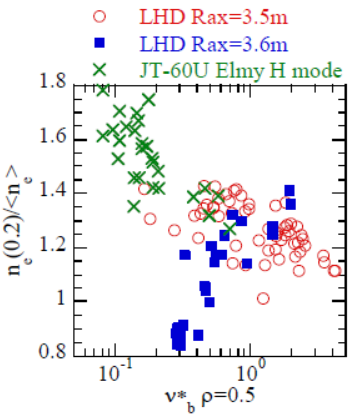

*Fig.2 Dependence of the density peaking factor on ν_b**

density peaking factor with decreasing collisionality [5]. In LHD at R_{ax}=3.5 m, density peaking factors moderately increased with decreasing ν^*_b as well and only peaked density profiles were observed. On the other hand, a different ν^*_b dependence was observed at 3.6 m where density peaking factors decreased with decreasing ν^*_b. Particle convection velocities for R_{ax}=3.6 m, which were estimated using a density-modulation experiment [3], were outwardly directed and close to neoclassical values at lower collisionality, suggesting that particle transport (thus the observed ν^*_b dependence shown in Fig. 2) was affected by neoclassical processes.

3. Response of turbulence with change of density profiles in JT-60U

In order to investigate the role of fluctuation on density peaking, density and NB power were scanned and fluctuation was measured in five discharges in the JT-60U campaign 2008. Figure 3 shows dependence of density peaking factor on effective collisionality (ν_{eff}), which was defined as the ratio of the electron–ion collision frequency to the curvature drift frequency[5]. At ν_{eff} <1, the linear Gyro kinetic theory predicts ITG/TEM can induce a peaked density profile [5]. The density peaking factor increased with a decrease of ν_{eff} as reported previously [2] and by other tokamak observations [5] suggesting the role of turbulence.

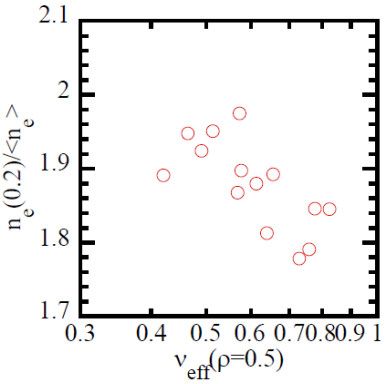

Fig.3 The dependence of the density peaking factor on ν_{eff} from JT-60U 2008 campaign. The data is from 14 cases of 5 discharges.

Figure 4 shows an example of temporal behavior in the data of Fig.3 showing NB power, normalized beta (β_N), line integrated density and the power spectrum of the reflectometer. The neutral beam power increases from 7.4 to 12.9MW in time as shown in Fig.4 (a). Figure 5 shows n_e and T_e profiles at low (7.4MW) and high NB power (12.9MW). The density and temperature profiles in Fig.5 (a) and (b) were accumulated during steady state (for 0.5~1s) in order to estimate their scale length accurately for the following analysis. Central line integrated density increases with the increase of NB power as shown in Fig.4 (b), however, the increase of the beam source is not a dominant effect as mentioned in the previous section. As shown in Fig.5 (a), the n_e profile became slightly peaked with higher NB power.

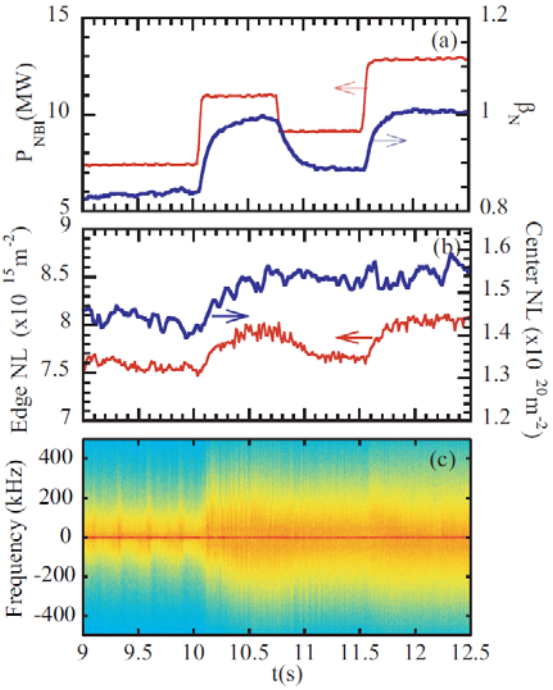

Fig.4 Time history of (a) NB power, notmalized beta (β_n), (b) line integrated density and (c)reflected power spectrum in JT-60U.

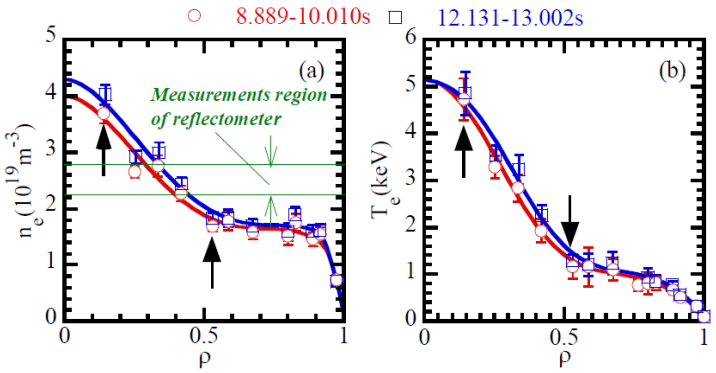

Fig.5 (a) n_e and (b) T_e profile at low (7.4MW, t=8.889-10.010s) and high (12.9MW, t=12.131-13.002s) NB power. Black arrows indicate YAG Thomson points when core scale length was calculated.

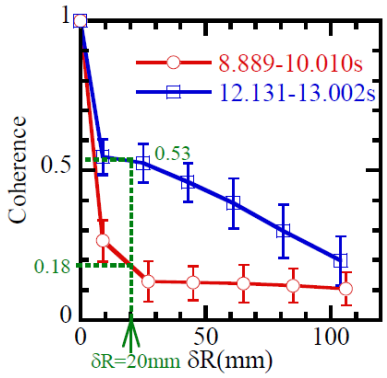

Fig.6 Radial coherence profile at high (7.4MW, t=8.889-10.010s) and low (12.9MW, t=12.131-13.002s) NB power. δR is the radial distance between the fixed and scanned channels.

The characteristics of turbulence were measured by an O mode correlation reflectometer [6] employing two close frequencies. One is fixed at 47.3GHz while the other is scanned 42.3-46.8GHz in 6 steps in time. Each step is 20ms, then the cross correlation of the reflected power was measured in 120msec for the density regimes 2.23-2.78x$10^{19}m^{-3}$. Figure 4 (c) shows time history of power spectrum of the fixed frequency channel. The power spectrum becomes broad after t=10s, when the NB power increased suggesting a change of turbulence characteristics. The measurement region is shown in Fig.5 (a).

Figure 6 shows the radial coherence of turbulence measured by the correlation reflectometer. Figure 6 was obtained from the accumulated data during steady state. Three and four frequency scan were possible for 8.889-10.010s and 12.131 -13.002s respectively. For each frequency scan, coherence was estimated for -200- -100kHz of a +-500kHz of heterodyne detection band width. The highest coherence was observed at -200 - -100kHz. In this frequency regime, the coherence has a distribution, thus, its averaged value was used as a representative value and its standard deviation was used as an error. Then, each average and standard deviation was averaged in the three scans for 8.889-10.010s and the four scans for 12.131-13.002s. The values of Fig.6 are an average of representative values of a series of scans. The error bars are the average of standard deviation of a series of scans.

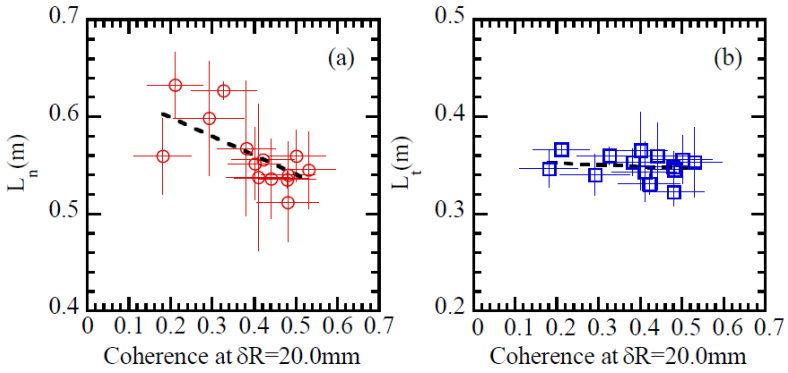

Fig.7 Relation between coherence at δR=20mm and (a) density and (b) temperature scale length.

As shown Fig6, there is a clear difference of the radial correlation of the turbulence between two timings. In the peaked density profile at 12.131-13.002s, the coherence was larger at the same radial separation of the cut off layer. This suggests the radial correlation is larger for a peaked density profile. For a more systematic study, the same analysis was applied to other cases in the data of Fig.3

The radial correlation was estimated as the coherence at the radial separation of cut off layer, which was 20mm. This definition was used since the coherence profile cannot be fitted well by using exponential function.

Since radial correlation is a local quantity, it was compared with the density and temperature scale lengths, which were defined as $L_n = -(1/n_e\ dn_e/dr)^{-1}$ and $l_t = -(1/T_e\ dT_e/dr)^{-1}$ respectively. Both scale lengths were estimated for the two points of YAG Thomson scattering, which are indicated by black arrows in Fig.5. These two points can show the scale length of the measurement region of the reflectometer. The error of the scale length is due to the error in the YAG Thomson scattering.

As shown in Fig.7 (a), the density scale length decreases with increase of coherence. On the other hand, no systematic trend is seen between coherence and temperature scale length. Figure 7 suggest a longer radial correlation is related to the density peaking.

The radial correlation length of turbulence can be the step size of diffusion, where turbulence can induce radial diffusion. So, Fig. 7(a) suggests diffusion is larger at a smaller L_n (more peaked profile). This is a clear contrast, radial correlation becomes smaller, then diffusion becomes smaller when an internal transport barrier is formed [7]. This is because the data set in this article is from the ELMy H mode. Any further confinement improvements were observed. Thus, with the increase of heating power, confinement degraded and diffusion increased.

The particle flux Γ is written as follows:

$$\Gamma = -D\nabla n_e + n_e V \tag{1}$$

In the plasma core region, the particle source can be negligible, then, in steady state, the particle flux can be zero. Then we obtain the following equation.

$$L_n = \frac{n_e}{\nabla n_e} = \frac{D}{V} \tag{2}$$

From eq. (2), it is clear that the increase of diffusion for more peaked density profile (smaller L_n) requires increase of inward directed pinch. Even for same L_n, an increase of D requires an

increase of inward directed V. In the ELMy H mode, a feedback loop may exist to increase the inward pinch associated with enhanced diffusion.

4. Response of turbulence with change of density profiles in LHD

The change of density profile with the temporal scan of P_{NB} is also observed in LHD. Figure 8 shows the temporal evolution of density, temperature and fluctuation behavior at R_{ax}=3.6m. At R_{ax}=3.6m, density peaking decreased with the decrease of collisionality in contrast to tokamak observation described in Sec.2. This dependence can be caused by the smaller anomalous contribution compared with R_{ax}=3.5m, and the larger neoclassical contribution compared with the tokamak. The fluctuations were measured by two-dimensional phase contrast imaging (2D-PCI) [8]. Local fluctuation power and local poloidal wavenumber can be measured. As shown in Fig.8 (a) and (b), electron density decrease, when the NB power increases after t=4.1sec. This is opposite response to the one observed in JT-60U, where density profile became more peaked with higher NB power as shown in Fig.5 (a).

As shown in Fig. 8 (d) and (e), fluctuation properties changed with the reduction of density. The measured phase velocity is poloidally directed and Doppler shifted by poloidal rotation. As shown in Fig 8 (d), the phase velocity inside last closed flux surface was directed to the electron diamagnetic (e-dia.) direction before the increase of NB power, then switched to the ion diamagnetic (i-dia.) direction after the increase of P_{NB}. According to the neoclassical radial electric field, the poloidal rotation was in the e-dia. direction due to a negative radial electric field during the whole discharge. Thus, the change of the poloidal phase velocity in the laboratory frame, indicates an increase of the i-dia. directed fluctuation phase velocity in plasma frame. As shown in Fig. 8 (e), core (ρ=0.-0.7) fluctuation power increased after an increase of P_{NB}.

Figure 9 shows the radial profile of the radial electric field (E_r), diffusion coefficient (D), convection velocity (V), n_e, T_e profiles and fluctuation profiles at low (1.1MW, at t=4.0s) and high (5.6MW, at t=4.5s) NB power. The experimental values of D and V were estimated from density modulation experiments in this discharge. The radial electric fields were estimated from the neoclassical ambipolar condition. The neoclassical values (E_r, D and V) were estimated from the GSRAKE

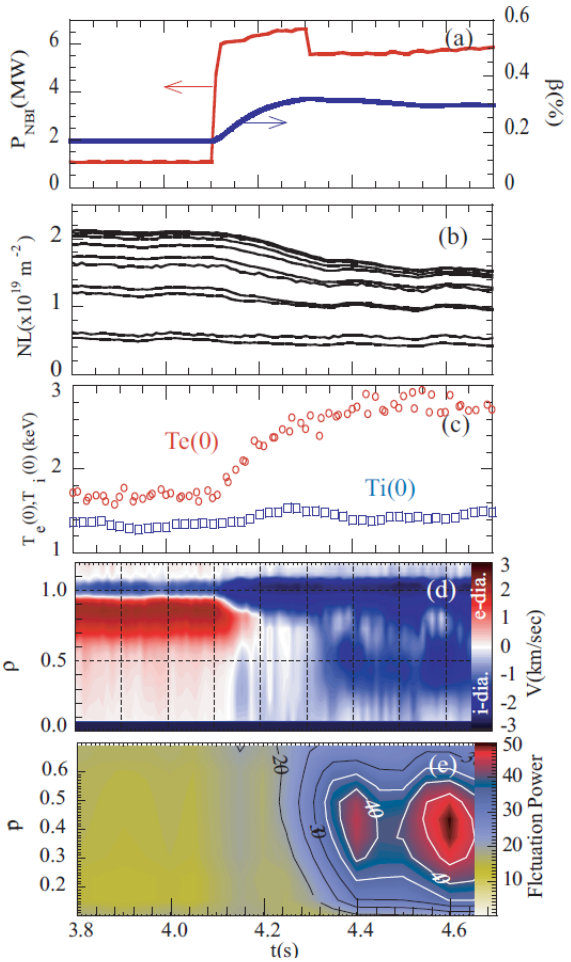

Fig.8 Time history of (a) NB heating power, diamagnetic β, and (b) line integrated denity. Higher values (upper trace) correspond to the chord close to magnetic axis. (c) central electron and ion temperature, (d) fluctuation phase velocity and (e) fluctuation power at ρ=0-0.7. R_{ax}=3.6m, Bt=2.75T. In Fig.8(d), red and blue colors indicate electron and ion diamagnetic directions in labolatory frame, respectively.

code [9]. In Fig.9 (g), (h), (i), three different neoclassical values are shown at ρ>0.5. These are the possible three roots of the neoclassical ambipolar condition.

As shown in Fig.9 (d) and (j), the n_e profiles changed from a peaked one to a hollow one. The change in D and V at ρ=0.4, where density reduced drastically, are summarized in Table.1.

The decrease of density peaking with the increase of P_{NB} is due to the increase of D and decrease of absolute V. It is in clear contrast to that in JT-60U where both D and V increased with an increase in P_{NB}. Also, the contribution of neoclassical D increased clearly. However, diffusion is dominated by anomalous diffusion after the increase of P_{NB} at t=4.5s as shown in Fig.9 (h). According to quasi linear gyrokinetic theory, diffusion coefficients are proportional to fluctuation power [10]. So, the increase of fluctuation power observed in Fig.8 (d) and Fig.9 (e),(k), can induce an increase of diffusion. So, increase of diffusion is partly due to the increase of neoclassical processes and partly due to the increase of anomalous processes. At R_{ax}=3.6m, previous results from wide range of P_{NB} scan (1~8MW) showed that the convection velocity was more or less comparable with the neoclassical calculations especially at lower collsionality and higher electron temperature [3,11,12]. It is likely that the change of convection velocity from inward with lower P_{NB} to outward with higher P_{NB} is due to the increase of neoclassical convection, because a neoclassical to be outward pinch was predicted outward in the whole region of the discharge.

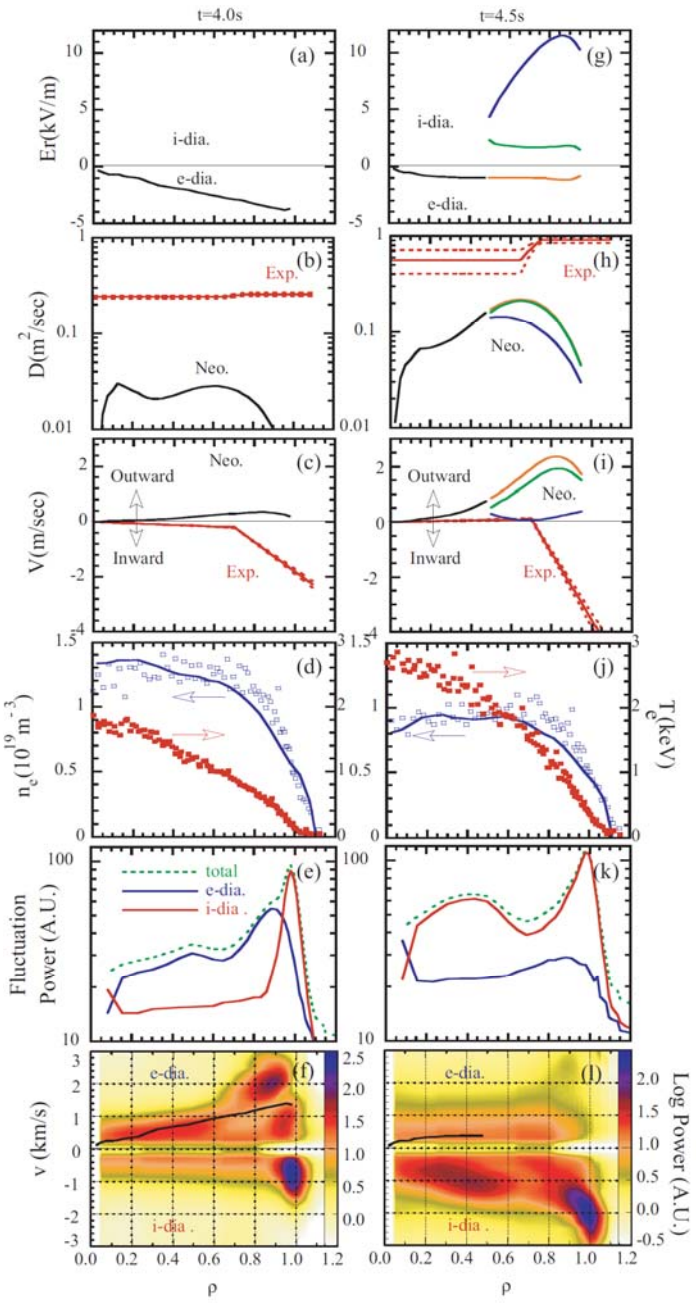

Fig.9(a), (g) Radial profile of E_r, (b), (h) D, (c),(i) V, (d),(j) n_e T_e, (e), (k) fluctuation power and (f), (l) fluctaution phase velocity. (a)-(f) are at low NB power (1.1MW at t=4.0s) and (g)-(l) are at high NB power (5.6MW at t=4.5s). Neoclassical E_rxB_t roation velocities are indicated by black lines in Fig.9 (f) and (l).

Both neoclassical and anomalous processes play roles in the change of the core density profile with the increase of P_{NB} in LHD. Turbulence can play a role in diffusion more than convection.

5. Summary

The changes of density profile and fluctuation characteristics were observed both in JT-60U and LHD. With a decrease of collisionality, the density profile became more peaked in JT-60U, while the density profile changed from peaked to a hollow profile in LHD

In both JT-60U and LHD, turbulence changed after changing density peaking suggesting a role on enhancement of diffusion. It is qualitatively suggested that an increase of diffusion induced an inward directed pinch in JT-60U, while the increase of outward neoclassical convection induce a decrease of the density peaking.

A detail comparison with linear and non linear modeling and an experimental survey in a wider region (different collisionality, different configurations including R_{ax}=3.5m of LHD) are required for further understanding.

The work in JT-60U was partly supported by the Grant-in-Aid for Young Scientists (A) 18686076, Japan Society for the Promotion of Science. The work in LHD was supported by NIFS research funding ULHH511.

	$D_{low\ power}$ (m^2/s)	$D_{high\ power}$ (m^2/s)	$D_{high\ power}/D_{low\ power}$	$V_{low\ power}$ (m/s)	$V_{high\ power}$ (m/s)	$V_{high\ power}/V_{low\ power}$
LHD_{total}	0.24	0.56	2.3	-0.12	0.06	-0.5
$LHD_{Neo.}$	0.02	0.12	6.0	0.12	0.49	4.1

Table 1 Comparison of D and V in LHD from density modulation experiments at ρ=0.4.

References

[1] YAMADA. H., et al., 2005 Nucl. Fusion 45 1684
[2] TAKENAGA, H., et al., 2008 Nucl. Fusion **48** 075004
[3] TANAKA KA, K., et al., 2007 Fusion Sci. Tech **51** 97
[4] MURAKAMI, S., et al., 2002 Nucl. Fusion **42** L19
[5] ANGIONI, C., et al., 2003 Phys. Plasmas **10** 3225
[6] OYAMA, N., *in preparation*
[7] TAKENAGA, H., et al., *this proceeding*
[8] TANAKA, K., et al., Rev. Sci. Instrum. in press
[9] BEIDLER, C. D., et al., 1995 Plasma Phys. Control. Fusion, **37**, 463
[10] WESSON, J., 2003 Tokamaks Third edition Oxford University press
[11] TANAKA, K., 2008 Nucl. Fusion 039801
[12] TANAKA, K., 2008 Plasma Fusion Res. 3, S1069